VSP

Advanced Robotics 23 (2009) 955–977

ADVANCED ROBOTICS
www.brill.nl/ar

Full paper

Attitude Estimation of a Biologically Inspired Robotic Housefly *via* Multimodal Sensor Fusion

Domenico Campolo [a,*], **Luca Schenato** [b], **Lijuan Pi** [c], **Xinyan Deng** [c] **and Eugenio Guglielmelli** [a]

[a] Biomedical Robotics Laboratory, Campus Bio-Medico University, 00128 Rome, Italy
[b] Department of Information Engineering, University of Padova, 35131 Padova, Italy
[c] Department of Mechanical Engineering, University of Delaware, Newark, DE 19716, USA

Received 8 August 2008; accepted 25 October 2008

Abstract
In this paper, we address sensor fusion for the attitude estimation of micromechanical aerial vehicles (MAVs), in particular a biologically inspired robotic housefly. First, a dynamic observer is proposed that estimates attitude based on kinematic data available from different and redundant bio-inspired sensors such as halteres, ocelli, gravitometers, magnetic compasses and light polarization compasses. In particular, following a geometric approach, the traditional structure of complementary filters, suitable for multiple sensor fusion, is specialized to the Lie group of rigid-body rotations $SO(3)$ and almost-global asymptotic stability is proved. Then, the filter performance is experimentally tested *via* a 3-d.o.f. robotic flapper and a custom-made set of inertial/magnetic sensors. Experimental results show good agreement, upon proper tuning of the filter, between the actual kinematics of the robotic flapper and the kinematics reconstructed from the inertial/magnetic sensors *via* the proposed filter.

Keywords
Sensor fusion, dynamic attitude estimation, biologically inspired robots

1. Introduction

There are presently several successful examples of autonomous flying vehicles, from airplanes [1] to helicopters [2]. However, their size hampers their use in surveillance and search-and-rescue missions in urban areas, in indoor environments and in natural disaster scenarios, such as after earthquakes. Therefore, there is an increasing need for very small size air vehicles with high performance. In partic-

* To whom correspondence should be addressed. E-mail: campolo@sssup.it

 DOI:10.1163/156855309X443052

ular, the current trend is to study micromechanical aerial vehicles (MAVs) using traditional air vehicle paradigms such as fixed-winged air vehicles [3] or rotorcrafts [4]. In contrast, inspired by the unmatched maneuverability and hovering capability by real insects such as the common housefly (*Musca domestica*), some groups have started using biomimetic principles to develop micromechanical flying insects (MFIs) with flapping wings that will be capable of sustained autonomous flight [5, 6].

The extraordinary performance of flying insects is the result of two peculiar features: (i) the enhanced unsteady-state aerodynamic forces and moments generated by the flapping wings [7–10], and (ii) the multimodal sensor fusion, i.e., the ability to integrate information from a number of different and redundant sensors to reduce the effect of noise and external disturbances [11–13].

In this paper, we focus explicitly on the latter feature of insect flight, i.e., on sensor fusion of redundant information for attitude control, and we assume that we can control directly the torque applied to the insect body as shown in Ref. [10]. The reason for focusing on orientation is that attitude stabilization is the first step towards overall flight control, as is clear from a vast amount of literature on helicopter stabilization [14].

Complementary and Kalman filters have traditionally been used to design attitude observers, especially in the presence of redundant measurements. Kalman filters work in the time domain focusing on the noise corrupting the signals and this leads to optimality when the noise is Gaussian. Complementary filters approach the problem from the frequency domain, falling in the category of the so-called Wiener filters, i.e., less general when it comes to dealing with noise. It should be noted, however, that in real applications such as navigation, assuming white, Gaussian noise is defintely a strong assuption. For linear systems, both types of filters may in fact lead to similar equations [15]. Although sensor fusion has been studied for decades and many results are available for linear spaces [16], it remains a hard problem on the Lie group of rigid-body rotations $SO(3)$ where standard tools like Kalman filtering cannot be applied directly.

Kalman filters were originally developed for linear systems and then extended to cope with nonlinearities *via* linearization techniques; nevertheless, they cannot guarantee global stability. On the other hand, complementary filters are capable of fully exploiting the rich nonlinear structure underlying problems such as rigid-body rotations, well described by the theory of Lie groups. Therefore, nonlinear complementary filters able to globally address stability properties of the proposed observer, i.e., taking into account the geometric features of $SO(3)$, in order to take advantage of powerful results such as the separation principle, proved by Maithripala *et al.* [17] to also hold on compact Lie groups such as the case of interest, will be a fundamental step towards attitude stabilization.

As the main contribution of this work, the traditional structure of complementary filters is specialized to the Lie group of rigid-body rotations $SO(3)$. In particular, a dynamic observer is proposed which derives an attitude estimate from redundant

information typically available from bio-inspired sensors. Following the geometric approach of Refs [18–20], this is achieved by avoiding the parametrization step. The proposed observer is based on a notion of state error which is intrinsic, so its performance does not depend on an arbitrary choice of coordinates, and coordinate-free, in the sense that the equations may be written explicitly without specifying coordinates for the configuration space.

As an experimental validation, the filter is used to reconstruct the kinematics of a 3-d.o.f. robotic flapper on which a suite a redundant inertial/magnetic sensors was assembled.

Section 2 reviews the navigation sensory system of real insects. In Section 3, a complementary filter for sensor fusion is proposed. In Section 4, the experimental validation of the filter performance is presented.

2. Sensory System of Flying Insects

One reason for superior performance exhibited by flying insects, besides the enhanced unsteady-state aerodynamic forces from flapping flight, is the highly specialized sensory system. In order to stabilize flight, insects can rely upon a number of different sensors. In the following, we briefly review a number of sensors available to insects for navigation, which represent a rich source of inspiration for the mechanical flying insect [21, 22].

2.1. Halteres

The halteres are club-shaped small appendages behind each wing that oscillate in anti-phase with respect of the wing, as shown in Fig. 1. The plane of oscillation is slightly tilted toward the tail of the insect to be able to measure Coriolis forces along all three body axes [23]. The halteres function as tiny gyroscopes and through

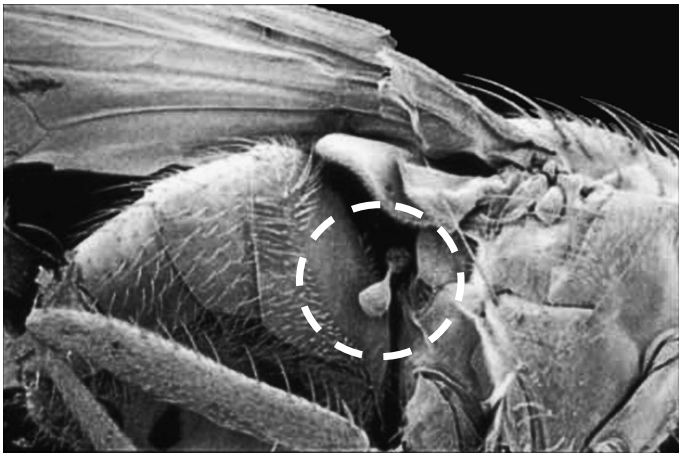

Figure 1. Photo of a fly haltere. Courtesy of Ref. [42].

appropriate signal processing [24] they can reconstruct the body angular velocity vector:

$$y_{\mathrm{hl}} = \omega. \tag{1}$$

The major drawback of halteres is that their measurements can be unpaired by body translational acceleration, which cannot be distinguished from the Coriolis forces. However, this problem can be alleviated by integrating angular velocities estimates from sensors such as the ocelli and the compound eyes visual system, which are immune from linear accelerations. Recently, preliminary prototypes of micro-electromechanical halteres have been fabricated and have shown promising results [25].

2.2. Mechanoreceptors

Insects wings and other parts of the body, such as the antennae, neck and legs, are innervated by campaniform sensilla. These nerves can sense and encode pressure forces when they are stretched or strained [26]. A large number of sensilla are located at the base of the wing to measure aerodynamic forces acting on the wings during motion and to elicit a compensatory mechanism to stabilize wing trajectory. In contrast, the sensilla on the legs can be used to measure the gravity acceleration, thus acting as a gravitometer. Therefore, we can assume that insect can measure the gravity vector with respect to the body frame, i.e.:

$$y_{\mathrm{g}} = R^{\mathrm{T}} g_0, \tag{2}$$

where g_0 are the (known) gravity vector components, measured with respect to the space frame. Similarly to the halteres, the mechanoreceptors are also affected by linear body accelerations (e.g., the antennae in moths act very similarly to halteres by measuring Coriolis's forces on mechanoreceptors placed at the base of the vibrating antennae [27]) and need to be integrated with other sensors.

2.3. Ocelli

The ocelli are three additional light-sensitive organs that look forward, leftward and rightward, respectively, located in the middle of the compound eyes as shown in Fig. 2, and provide signals that are used for stabilization with respect to rapid perturbations in roll and pitch [21]. In fact, these sensor can estimate the position of the sun with respect to the insect body by comparing the signals from the left and right ocelli to estimate the roll angle, and by comparing the signal from the forward-looking ocellus with the mean of the signals from the left and the right ocelli to estimate the pitch angle [28].

2.4. Compound Eyes

The compound eyes of the insects provide different types of signals needed for the optomotor systems. They provide computation of insect angular velocities accomplished by using large-field neurons that are tuned to respond to the specific patterns of optic flow that are generated by yaw, roll and pitch [29]. Differently from hal-

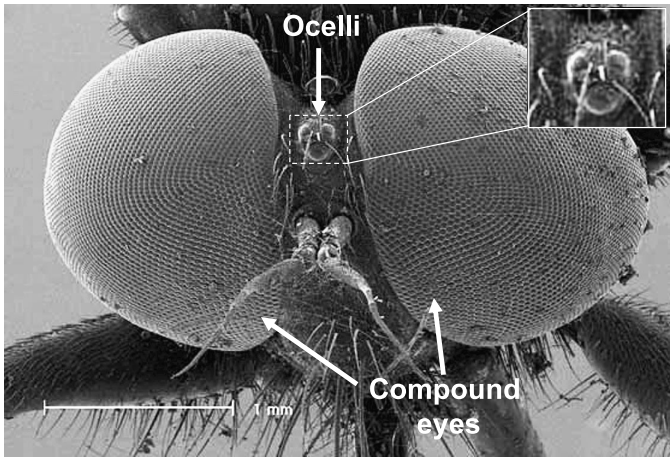

Figure 2. Photo of a fly's head showing the compound eyes and the ocelli with its three photoreceptors. Courtesy of Ref. [43].

teres, these estimates require longer signal processing periods, but are not affected by linear accelerations. In other words, compound eyes precisely estimate angular velocities at low frequencies.

The compound eyes can also estimate body orientation and position by higher-level visual processing like object fixation and landmarks detection. Although this signal processing requires even longer times, it can provide useful position information at low frequency for navigation and path planning [13].

Finally, the dorsally directed (upward-looking) regions of the compound eyes of many insects are equipped with specialized photoreceptors that are sensitive to the polarized light patterns that are created by the sun in the sky. These photoreceptors feed into polarization-sensitive interneurons that function as 'celestial compasses', informing the insect about the direction in which it is flying in relation to the sky's polarization pattern. The polarization-sensitive system is used by insects to establish and maintain the correct heading direction whilst navigating toward a distant goal. In other words, insects can measure their orientation relative to the direction of the light polarization: $p_0 \in \mathbb{R}^3$, as:

$$y_{\mathrm{p}} = R^{\mathrm{T}} p_0. \tag{3}$$

Differently from the ocelli, the light polarization direction is not affected by light intensity. In fact, while estimation of sun position using the ocelli can be impaired when passing from a shaded region to a sunny region, the estimation of polarization direction is unaffected. Bio-inspired polarized light compasses have been successfully fabricated and used for robot navigation [30].

2.5. Magnetic Compass

Recent studies indicate that some insects also possess a magnetic sense that informs them of their heading direction and helps them maintain it [31]. Similarly to the

light polarization sensor, we can argue that insects can measure the components of the magnetic field with respect to the body as follows:

$$y_{\mathrm{m}} = R^{\mathrm{T}} b_0, \tag{4}$$

where $b_0 \in \mathbb{R}^3$ is the direction of the magnetic field relative to the space frame. A possible electromechanical implementation of a magnetic compass suitable for small-size vehicles is given in Ref. [32].

3. Sensor Fusion *via* Complementary Filters

The sensory system of real insects is clearly redundant, e.g., kinematic quantities such as the angular velocity are derived from more than one sensor. Information from different sensors is then 'fused' together.

Complementary filters traditionally arise in applications where redundant measurements of the same signal are available [16] and the problem is combining all available information in order to minimize the instrumentation error.

For the sake of simplicity, consider only two sensors, s_1 and s_2, providing readings of the same quantity, e.g., the angular velocity ω, with different noise characteristics, i.e., $s_1 = \omega + n_1$ and $s_2 = \omega + n_2$, where $\|n_1\| < \|n_2\|$ at high frequency, while $\|n_2\| < \|n_1\|$ at low frequency. Then a low-pass filter $L(s)$ and its complementary high-pass filter $H(s) = 1 - L(s)$ can be used to fuse information:

$$s_{\mathrm{fusion}} = s_1 H(s) + s_2 L(s) = \omega + n_2 L(s) + n_1(1 - L(s)), \tag{5}$$

from two or more sensors (e.g., halteres, ocelli and compound eyes). The cut-off frequency of the filter $L(s)$ can be chosen so that the spectral content of $n_2 L(s) + n_1(1 - L(s))$ will be less than the spectral content of n_1 or n_2 [16].

Remark 1 (non-dynamic estimation). *The kinematic variable is dynamically unaffected by the filter. The estimated variable (i.e., the output of the filter) is related to the input variable* via *a purely algebraic relation in the time domain and no dynamics are involved in the noiseless case.*

Such filters can be safely used in feedback loops to fuse readings of the same kinematic variable from different sensors since no extra dynamics is added to the overall system and stability (which involves noiseless conditions) is not affected.

Complementary filters can be generalized to fuse information deriving from sensors when the sensed variables are related by differential equations, e.g., position and speed. In these cases, the filter introduces some dynamics between the estimated output and the sensed inputs.

The differential equations relating the sensed variables may be nonlinear; this is typically the case when attitude is concerned. The theory of complementary and Kalman filters has been traditionally used to design attitude filters. Although the Kalman filters can be extended (EKF) to nonlinear cases, they fail in capturing the

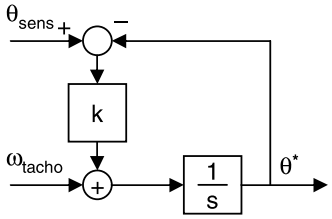

Figure 3. Linear complementary filter for a rotational mechanical system with 1 d.o.f.

nonlinear structure of the configuration space of problems involving, for example, rotations of a rigid body, and most importantly, they can run into instabilities. On the other hand, nonlinear filters [33], in particular complementary filters, can better capture such a nonlinear structure.

3.1. Dynamic Attitude Estimation

As an example of use of complementary filters when different kinematic variables are involved, consider the linear case of a rotational mechanical system with 1 d.o.f. (θ). As shown in Ref. [16], complementary filters such as the one represented in Fig. 3 are traditionally used to fuse information available from both angular position sensors and tachometers, θ_{sens} and ω_{tacho}, respectively. Let θ^* be the estimate of θ. The filter gain k in Fig. 3 determines the transition frequency of the filter after which the data from the tachometer (ω_{tacho}) are weighted more, whereas before the transition frequency data from the position sensors (θ_{sens}) are predominant on the dynamic equation (the integrator $1/s$). The optimal value for k is in fact determined by the characteristics of measurement noise, see Ref. [16].

Differently from the previous example, $SO(3)$ is a nonlinear space and that is where the advantages of a geometric approach can be fully appreciated. Apart from nonlinear dynamics, the very definition of estimation error requires caution. In the linear case $e = \theta - \theta^*$ is a typical choice while quantities such as $R - R^*$ with R, $R^* \in SO(3)$ are no longer guaranteed to belong to $SO(3)$. Following Ref. [34], the estimation error will be defined as $E = R^{\mathrm{T}} R^*$.

Next, a complementary filter on $SO(3)$ for dynamic attitude estimation is presented that fuses information from gyroscopes, and from different and possibly redundant navigation sensors, such as the ones described in Section 2.

3.2. Complementary Filtering on SO(3)

Consider $N \geqslant 2$ homogenous and time-invariant vector fields $\vec{v}_1, \vec{v}_2, \ldots, \vec{v}_N$ (e.g., the gravitational field, the geomagnetic field, the light direction, etc.) without the need, for the moment, to specify their components (therefore, the symbol $\vec{\cdot}$). Assume that at least two of them (e.g., $\vec{v}_1$ and $\vec{v}_2$, without loss of generality) are independent; this can be expressed in a form that is invariant and coordinate-free:

$$\vec{v}_1 \times \vec{v}_2 \neq 0. \tag{6}$$

Definition 1. *Given a rigid body, define a body frame $\mathcal{B}$ on it. Let the rigid body be at rest at some time t_0 and define, thus, a space frame $\mathcal{S}_0$ as the one coincident with the body frame $\mathcal{B}$ at time t_0. Let the constant vectors $v_{i0} = [v_{i0x} \;\; v_{i0y} \;\; v_{i0z}]^{\mathrm{T}}$ represent the components of each vector field at time t_0 as measured by a set of sensors on the rigid body. At any time t, let $R(t) : \mathbb{R} \to SO(3)$ be a twice-differentiable function representing the orientation of the rigid body in 3-D space with respect to the space frame $\mathcal{S}_0$, let $v_i = [v_{ix} \;\; v_{iy} \;\; v_{iz}]^{\mathrm{T}}$ be the (time-variant) components of each field and let ω_{gyr} be readouts of the gyroscopes; both v_i and ω_{gyr} are referred to the (body) moving frame.*

Before presenting the main theorem concerning the proposed observer and its convergence properties, two lemmas are presented that relate the influence of the current attitude R on the sensor measurements v_i as well as the role of gyroscopes in navigation.

Lemma 1. *The trajectory $R(t) \in SO(3)$, defined as in Definition* 1*, is reflected in the measurements of the gyroscopes and of the vector fields sensors and can be expressed as*

$$\begin{cases} \widehat{\omega}_{\mathrm{gyr}} = R^{\mathrm{T}} \dot{R} = \widehat{\omega} \\ v_i = R^{\mathrm{T}} v_{0i}. \end{cases} \tag{7}$$

See proof in the Appendix.

Lemma 2. *Let $R(t) : \mathbb{R} \to SO(3)$ represent, as in Definition* 1*, the trajectory on $SO(3)$ of a rigid-body embedding a set of gyroscopes and let the angular velocity ω of the rigid body be available, as in* (7)*,* via *readings from such gyroscopes. Let $R^{*\mathrm{T}} \dot{R}^* = \widehat{\omega}$ denote the dynamics of an estimator, then the tracking error:*

$$E \triangleq R^{\mathrm{T}} R^* \tag{8}$$

is such that $\|E(t)\|_{SO(3)} =$ constant. *In particular, the following identity holds:*

$$\langle\langle \log(E), -E^{\mathrm{T}} \widehat{\omega} E + \widehat{\omega} \rangle\rangle_{so(3)} = 0. \tag{9}$$

See proof in the Appendix.

Lemma 2 simply states that gyroscopes, in fact, are not necessary for stability, for which the measurements of at least two vector fields such as the gravitational and the geomagnetic ones are sufficient [35], but knowledge of the angular velocity is beneficial for performance, especially when disturbances are present. Therefore, the proposed filter can be still used for stable tracking when the information from gyroscopes is completely or partially missing (e.g., only mono-axial or bi-axial gyroscopes are available, as for the case of the halteres), of course with a worsening of the performance.

Theorem 1. *Let $R(t):\mathbb{R}\to SO(3)$ represent the orientation of the rigid body as in Definition* 1. *Let $R^*(t)$ denote the estimate of $R(t)$ and let it be defined by the following observer:*

$$\begin{cases} \dot{R}^* = R^*\widehat{\omega}^* \\ \omega^* = \omega_{\text{gyr}} + \sum_{i=1}^{N} k_i (v_i \times v_i^*) \\ v_i^* = R^{*\text{T}} v_{0i}, \end{cases} \tag{10}$$

where $k_i > 0$ are the filter gains, and ω_{gyr} and v_i represent the sensor readings as in (7).

The observer (10) *asymptotically tracks $R(t)$ for almost any initial condition $R^*(0) \neq R(0)$ and in particular:*

$$\lim_{t\to\infty} R^{\text{T}}(t) R^*(t) = I. \tag{11}$$

See proof in the Appendix.

Theorem 1 is stated in a form which is similar to Ref. [36], but our proof, which extends our previous work [35], is in line with Refs [17, 20]. In particular, we adopt a geometric approach that allows applying separation principle as in Refs [17, 20], proved to hold for compact Lie groups as $SO(3)$, the case of interest. The aim is to prove that our proposed observer can provide a robust estimation of orientation to be used for attitude stabilization, which will be described in a forthcoming paper.

4. Experimental Results

In this section, the experimental results relative to attitude estimation of the end-effector of a robotic flapper are presented.

4.1. Experimental Setup

A robotic wrist was designed to generate motion in 3 independent rotational d.o.f. A bevel gear wrist mechanism was developed to transmit the motion of coaxial drive shafts to the plate holder as shown in Fig. 4. The roll and pitch ranges do not have any limits, but the yaw angle was constrained to 45° in our mechanical wrist. Drive shafts were powered by Maxon 16 mm DC brush motors with planetary gearheads and magnetic encoders. Gearhead reductions were 19:1 for yaw and pitch, and 84:1 for roll. All three motors have been upgraded to 84:1 gearheads. The mechanism itself saw gear ratios (drive to driven) of 4:1 for roll, 8:1 for yaw and 1:1 for pitch. The wrist mechanism was reduced in size (roughly 3.81 cm × 3.81 cm × 3.18 cm) to accommodate greater motion. A parallel plate mounting structure for the motors makes the setup compact and portable (see Fig. 4). The design allows for quick and easy changing of the sensor plate. The motors were driven from MATLAB Simulink models, which used an additional toolbox provided by the control board manufacturer (Quanser Consulting) to communicate with the hardware. PID controllers were used to run the motors at a high level of precision: up to a $1/10°$. Motion commands from the computer were amplified by analog amplifier

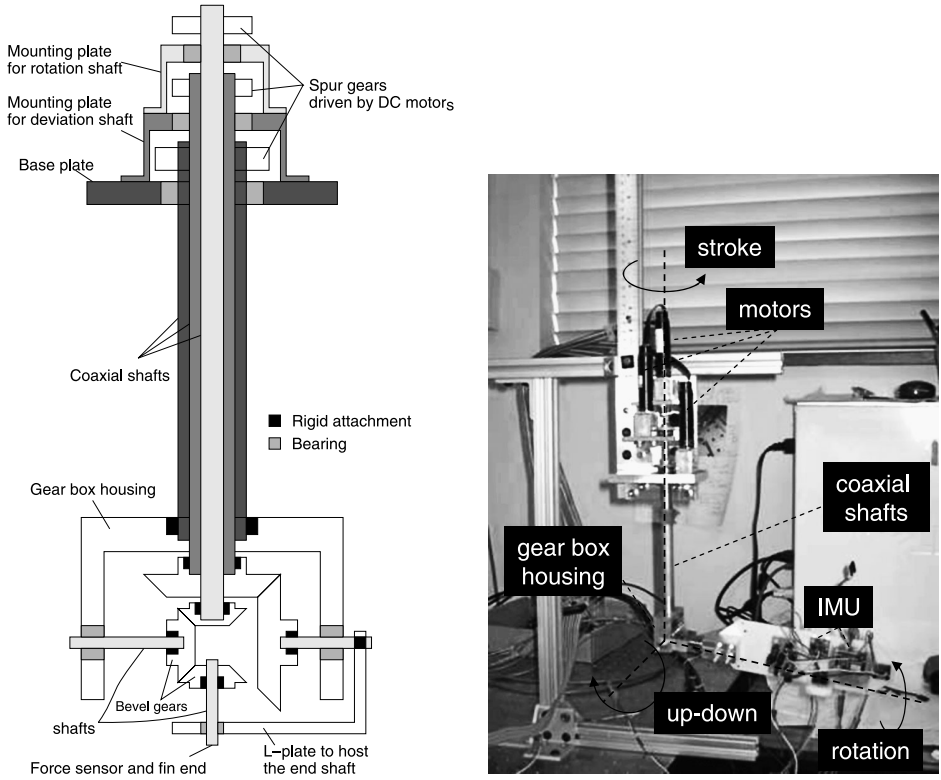

Figure 4. First-generation 3-d.o.f. mechanical flapper. (Left) Design layout (not to scale). (Right) Actual implementation comprising the assembled inertial magnetic unit (IMU).

units (Advanced Motion Control) running in torque mode, which directly controls the input current that the motor receives in order to perform a given motion.

As for the sensors, we used the Honeywell HMC2003 high-sensitivity, three-axis magnetic sensor to measure low magnetic field strengths, such as the geomagnetic field. The sensitivity is 1 V/Gauss and the bandwidth is 1 kHz. The micro accelerometer we used is ADXL330 (Analog Devices), which is a small, thin, low-power three-axis accelerometer with signal-conditioned voltage outputs all on a single monolithic IC. It measures acceleration with range of up to 3 g. It can measure the static acceleration of gravity, as well as dynamic acceleration resulting from motion. Bandwidth has a range of 0.5–1600 Hz for the x- and y-axes, and a range of 0.5–550 Hz for the z-axis. The sensitivity of each axis is 300 mV/Gauss with good linearity. For the angular rate sensor, we used IDG-300 (InvenSense), an integrated two-axis angular rate sensor (gyroscope). Two chips of IDG-300 were used to make a three-axis gyroscope system and the bandwidth is 140 Hz.

4.2. Results

The sensors were assembled and mounted on the plate attached to the robotic wrist. Angular motions in roll, pitch and yaw were performed independently, real-time

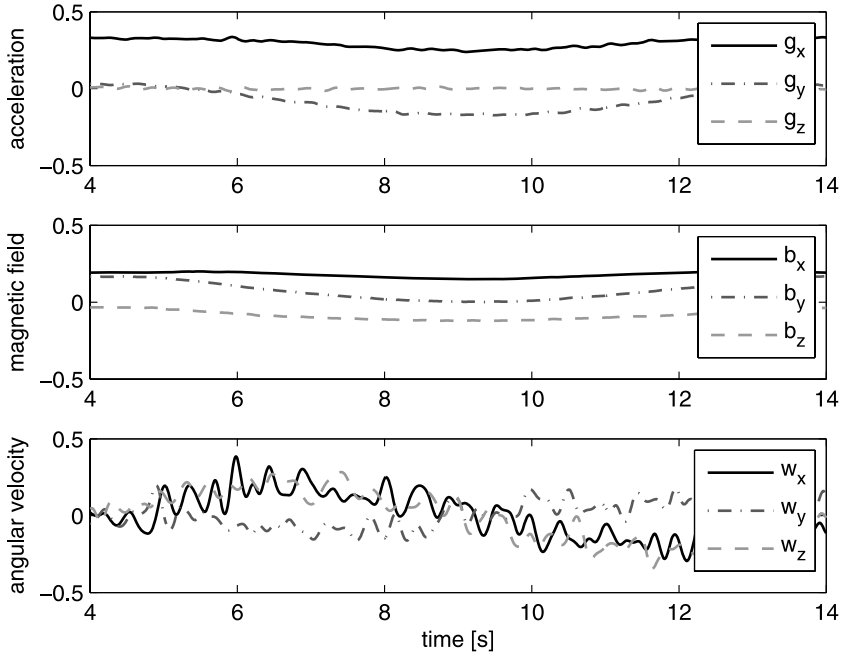

Figure 5. Normalized calibrated data from sensors. Acceleration and magnetic field are normalized with respect to the Earth's gravitational and the geomagntic fields. Angular velocity is normalized with respect to 0.11 rad/s (maximum value obtained in the performed experiment).

sensor output was obtained from the data acquisition systems, and the sensor fusion algorithm results are compared with the actual wrist motion (read from the motor encoder).

Coupled motions with multiple degrees of freedom were also performed and calibrated data from sensors derived from a particular motion are shown in Fig. 5. Experimental results are promising in the sense that the actual motion can be reconstructed after proper tuning of the filter (i.e., after choosing appropriate gain values). Figure 6 shows how the commands given to the high-precision servo-motors (ϕ, α and β) of the robotic flapper can be estimated. Note that, due to the mechanical coupling of the 3-d.o.f. mechanical flapper, only two motors need to be driven in order to produce a 3-D motion of the fin.

Also, in Fig. 5, the actual sensor data from the test show high-frequency oscillations, which is due to the plate vibration during acceleration; this can be reduced by mounting the sensors on a shorter plate, therefore, reducing the load induced torque on the gearbox.

5. Conclusions

In this work, we present a geometric, i.e., intrinsic and coordinate-free, approach to attitude estimation of a MFI, derived from multiple and possibly redundant bio-

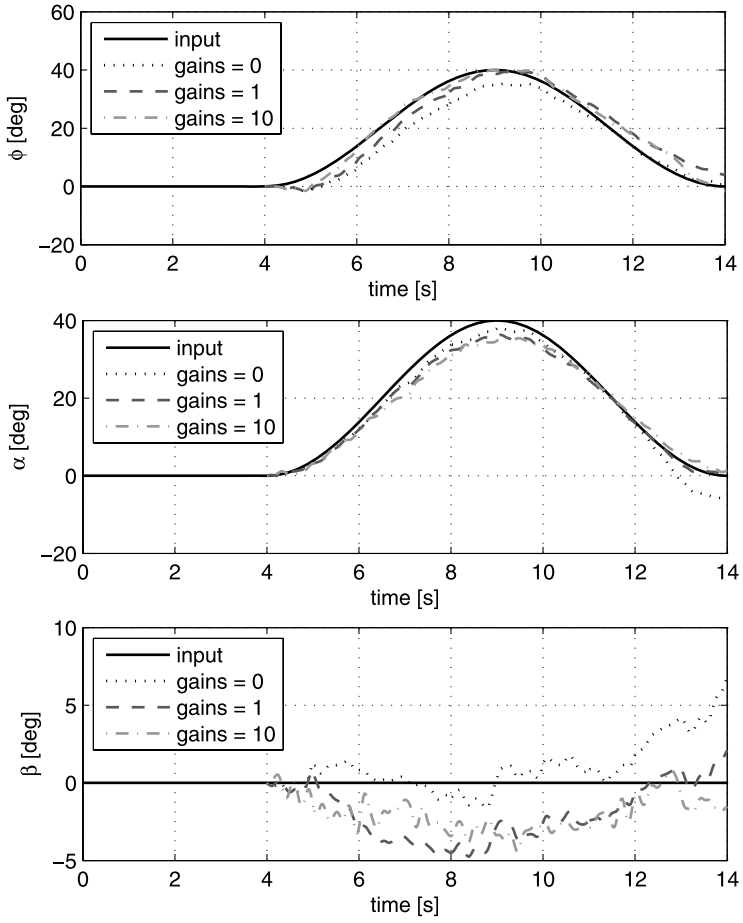

Figure 6. Angular motions (ϕ, α and β) of each of the three high-precision servo-motors (the solid line denotes the input command to the motor) can be reconstructed from calibrated data *via* the complementary filter algorithm.

inspired navigation sensors. Such a multimodal sensor fusion is implemented by a dynamic observer; in particular, a complementary filter is proposed that is specialized to the nonlinear structure of the Lie group of rigid-body rotations.

The proposed filter is experimentally tested. In particular, a 3-d.o.f. robotic flapper is used to generate a known trajectory. A custom-made suite of inertial/magnetic sensors was assembled on the end-effector of the robotic flapper and the filter was used to estimate the actual (known) motion of the robotic flapper.

The attitude observer presented in this work can robustly be used for attitude stabilization. In particular, the property of almost-global stability on the configuration space of rigid-body orientations is fundamental to invoke the separation principle that decouples the attitude estimation problem from the attitude control problem, but this will be part of future work where the proposed filter will be used to stabilize

the attitude of robotic platforms such as small flying vehicles as well as biomimetic swimming robots.

References

1. J. P. How, E. King and Y. Kuwata, Flight demonstrations of cooperative control for UAV teams, in: *Proc. AIAA 3rd Unmanned Unlimited Technical Conf.*, Chicago, IL, pp. 1509–1516 (2004).
2. H. J. Kim, D. H. Shim and S. Sastry, A flight control system for aerial robots: algorithms and experiments, *Control Eng. Pract.* **11**, 1389–1400 (2003).
3. J. Grasmeyer and M. T. Keennon, Development of the black widow micro air vehicle, in: *Proc. 39th AIAA Aerospace Sciences Meeting and Exhibit*, Reno, NV, AIAA-2001-0127 (2001).
4. I. Kroo and P. Kunz, Development of the mesicopter: a miniature autonomous rotorcraft, in: *Proc. American Helicopter Society Vertical Lift Aircraft Design Conf.*, San Francisco, CA (2000).
5. R. S. Fearing, K. H. Chiang, M. H. Dickinson, D. L. Pick, M. Sitti and J. Yan, Wing transmission for a micromechanical flying insect, in: *Proc. of IEEE Int. Conf. on Robotics and Automation*, San Francisco, CA, pp. 1509–1516 (2000).
6. R. C. Michelson and M. A. Naqvi, Beyond biologically inspired insect flight, in: *Proc. von Karman Institute for Fluid Dynamics RTO/AVT Lecture Series on Low Reynolds Number Aerodynamics on Aircraft Including Applications in Emergening UAV Technology*, Brussels, pp. 1–19 (2003).
7. S. P. Sane and M. H. Dickinson, The control of flight force by a flapping wing: lift and drag production, *J. Exp. Biol.* **204**, 2607–2626 (2001).
8. S. P. Sane, The aerodynamics of insect flight, *J. Exp. Biol.* **206**, 4191–4208 (2003).
9. G. K. Taylor, Mechanics and aerodynamics of insect flight control, *Biol. Rev.* **76**, 449–471 (2001).
10. X. Deng, L. Schenato and S. S. Sastry, Flapping flight for biomimetic robotic insects. Part II: flight control design, *IEEE Trans. Robotics* **22**, 789–803 (2006).
11. L. Schenato, W. C. Wu and S. S. Sastry, Attitude control for a micromechanical flying insect *via* sensor output feedback, *IEEE Trans. Robotics Automat.* **20**, 93–106 (2004).
12. J. Wessnitzer and B. Webb, Multimodal sensory integration in insects: towards insect brain control architectures, *Bioinspirat. Biomimet.* **1**, 63–75 (2006).
13. M. Epstein, S. Waydo, S. B. Fuller, W. Dickson, A. Straw, M. H. Dickinson and R. M. Murray, Biologically inspired feedback design for drosophila flight, in: *Proc. IEEE American Control Conf.*, New York, NY, pp. 3395–3401 (2007).
14. G. J. Leishman, *Principles of Helicopter Aerodynamics*. Cambridge University Press, Cambridge (2000).
15. W. T. Higgins, A comparison of complementary and Kalman filtering, *IEEE Trans. Aerospace Electon. Syst.* **11**, 321–325 (1975).
16. R. G. Brown and P. Y. C. Hwang, *Introduction to Random Signals and Applied Kalman Filtering*. Wiley, New York, NY (1992).
17. D. H. S. Maithripala, J. M. Berg and W. P. Dayawansa, Almost-global tracking of simple mechanical systems on a general class of Lie groups, *IEEE Trans. Automatic Control* **51**, 216–225 (2006).
18. D. E. Koditschek, The application of total energy as a Lyapunov function for mechanical control systems, *Dyn. Control Multibody Syst.* **97**, 131–157 (1989).
19. F. Bullo and R. M. Murray, Tracking for fully actuated mechanical systems: a geometric framework, *Automatica* **35**, 17–34 (1999).
20. D. H. S. Maithripala, J. M. Berg and W. P. Dayawansa, An intrinsic observer for a class of simple mechanical systems on a Lie group, *SIAM J. Control Optim.* **44**, 1691–1711 (2005).

21. J. Chahl, Bioinspired engineering of exploration systems: a horizon sensor/attitude reference system based on the dragonfly ocelli for Mars exploration applications, *J. Robotic Syst.* **20**, 35–42 (2003).
22. X. Deng, L. Schenato, W. C. Wu and S. S. Sastry, Flapping flight for biomimetic robotic insects. Part I: system modeling, *IEEE Trans. Robotics* **22**, 789–803 (2006).
23. R. Hengstenberg, Mechanosensory control of compensatory head roll during flight in the blowfly *Calliphora erythrocephala*, *J. Comp. Physiol. A* **163**, 151–165 (1988).
24. G. Nalbach, The halteres of the blowfly *Calliphora*: I. Kinematics and dynamics, *J. Comp. Physiol. A* **173**, 293–300 (1993).
25. W. C. Wu, R. J. Wood and R. F. Fearing, Halteres for the micromechanical flying insect, in: *Proc. IEEE Int. Conf. on Robotics and Automation*, Washington, DC, pp. 60–65 (2002).
26. M. H. Dickinson, Linear and nonlinear encoding properties of an identified mechanoreceptor on the fly wing measured with mechanical noise stimuli, *J. Exp. Biol.* **151**, 219–244 (1990).
27. S. P. Sane, A. Dieudonne, M. A. Willis and T. L. Daniel, Antennal mechanosensors mediate flight control in moths, *Science* **315**, 863–866 (2007).
28. H. Schuppe and R. Hengstenberg, Optical properties of the ocelli of *Calliphora erythrocephala* and their role in the dorsal light response, *J. Comp. Biol. A* **173**, 143–149 (1993).
29. W. Reichardt and M. Egelhaaf, Properties of individual movement detectors as derived from behavioural experiments on the visual system of the fly, *Biol. Cybernet.* **58**, 287–294 (1988).
30. D. Lambrinos, H. Kobayashi, R. Pfeifer, M. Maris, T. Labhart and R. Wehner, An autonomous agent navigating with a polarized light compass, *Adaptive Behavior* **6**, 131–161 (1997).
31. E. Wajnberga, G. Cernicchiaroa, D. Acosta-Avalosb, L. J. El-Jaicka and D. M. S. Esquivel, Induced remanent magnetization of social insects, *J. Magnet. Magnet. Mater.* **226–230**, 2040–2041 (2001).
32. W. C. Wu, L. Schenato, R. J. Wood and R. F. Fearing, Biomimetic sensor suite for flight control of MFI: design and experimental results, in: *Proc. IEEE Int. Conf. on Robotics and Automation*, Taipei, pp. 1146–1151 (2003).
33. F. Daum, Nonlinear filters: beyond the Kalman filter, *IEEE A&E Syst. Mag.* **20**, 57–69 (2005).
34. F. Bullo and R. F. Murray, Proportional derivative (PD) control on the Euclidean group, *Technical Report*, California Institute of Technology, Anaheim, CA (1995).
35. D. Campolo, F. Keller and E. Guglielmelli, Inertial/magnetic sensors based orientation tracking on the group of rigid body rotations with application to wearable devices, in: *Proc. IEEE/RSJ Int. Conf. on Intelligent Robots and Systems*, Beijing, pp. 4262–4267 (2006).
36. T. Hamel and R. Mahony, Attitude estimation on $SO(3)$ based on direct inertial measurements, in: *Proc. IEEE Int. Conf. on Robotics and Automation*, Orlando, FL, pp. 2170–2175 (2006).
37. V. I. Arnold, *Mathematical Methods of Classical Mechanics*, 2nd edn. Springer, New York, NY (1989).
38. T. Frankel, *The Geometry of Physics: An Introduction*. Cambridge University Press, Cambridge (1997).
39. R. M. Murray, Z. Li and S. S. Sastry, *A Mathematical Introduction to Robotic Manipulation*. CRC Press, Boca Raton, FL (1994).
40. S. S. Sastry, *Nonlinear Systems: Analysis, Stability and Control*. Springer, New York, NY (1999).
41. F. Bullo and A. D. Lewis, *Geometric Control of Mechanical Systems*. Springer, New York, NY (2005).
42. Commonwealth Scientific and Industrial Research Organisation. Available at: http://www.csiro.au
43. Victoria Museum. Available at: http://www.museum.vic.gov.au

Appendix A. Mathematical Background

This section briefly describes the notation and several geometric notions that will be used throughout the paper. For additional details, the reader is referred to texts such as [37–41].

A.1. Basic Definitions

As shown in Refs [37, 39], the natural configuration space for rigid-body orientations is the Lie group $SO(3)$:

$$SO(3) = \{R \in \mathbb{R}^{3\times 3} : R^{\mathrm{T}}R = I, \det R = 1\}.$$

Consider now the coordinate frames $\mathbb{R}^3_{\mathrm{S}}$ and $\mathbb{R}^3_{\mathrm{B}}$:

- $\mathbb{R}^3_{\mathrm{S}} \approx \mathbb{R}^3$: the space coordinate frame, or initial configuration frame.
- $\mathbb{R}^3_{\mathrm{B}} \approx \mathbb{R}^3$: the body frame, which is attached to the body (this can be thought of as defined by the sensors-sensitive axis), initially coincident with the space frame.

An element R of $SO(3)$ can be thought of as a map from the body frame to the space frame, i.e., $R : \mathbb{R}^3_{\mathrm{B}} \to \mathbb{R}^3_{\mathrm{S}}$.

A trajectory of the rigid body is the curve $R(t) : \mathbb{R} \to SO(3)$. The velocity vector $\dot{R}$ is tangent to the group $SO(3)$ in R but, as shown in Refs [37, 39], rather than considering $\dot{R}$, two important quantities are worth considering:

- $\dot{R}R^{\mathrm{T}}$: representing the rigid-body angular velocity relative to the space frame.
- $R^{\mathrm{T}}\dot{R}$: representing the rigid-body angular velocity relative to the body frame.

These are both elements of the Lie algebra $so(3)$, i.e., the tangent space to the group $SO(3)$ at the identity I. Elements of the Lie algebra are represented by skew-symmetric matrices.

In the case of $SO(3)$, there exists [39] an isomorphism of vector spaces $\hat{\cdot} : so(3) \to \mathbb{R}^3$, referred to as hat operator, that allows writing $so(3) \approx \mathbb{R}^3$. For a given vector $a = [a_1 \;\; a_2 \;\; a_3]^{\mathrm{T}} \in \mathbb{R}^3$, we write:

$$\hat{\cdot} : a = \begin{bmatrix} a_1 \\ a_2 \\ a_3 \end{bmatrix} \longrightarrow \begin{bmatrix} 0 & -a_3 & a_2 \\ a_3 & 0 & -a_1 \\ -a_2 & a_1 & 0 \end{bmatrix} = \hat{a}. \tag{A.1}$$

Denote $(\cdot)^{\vee} : \mathbb{R}^3 \to so(3)$ its inverse, referred to as the vee operator:

$$(\cdot)^{\vee} : \hat{a} = \begin{bmatrix} 0 & -a_3 & a_2 \\ a_3 & 0 & -a_1 \\ -a_2 & a_1 & 0 \end{bmatrix} \longrightarrow \begin{bmatrix} a_1 \\ a_2 \\ a_3 \end{bmatrix} = (\hat{a})^{\vee}. \tag{A.2}$$

The Lie algebra is equipped with an operator, the Lie brackets $[\cdot, \cdot]$, which is defined by the matrix commutator:

$$[\hat{a}, \hat{c}] = \hat{a}\hat{c} - \hat{c}\hat{a} = \widehat{a \times c}, \tag{A.3}$$

where $a, c \in \mathbb{R}^3$, $\hat{a}, \hat{c} \in so(3)$ and $\times$ is the cross-product in $\mathbb{R}^3$.

Given a finite-dimensional vector space V, let V^* be its dual space, i.e., the space whose elements (covectors) are linear functions from V to $\mathbb{R}$. If $\sigma \in V^*$, then $\sigma : V \to \mathbb{R}$. Denote the value of σ on $v \in V$ by $\langle \sigma, v \rangle$, i.e., the pairing operator $\langle \cdot, \cdot \rangle : V^* \times V \to \mathbb{R}$.

If $V = \mathbb{R}^n$ then $V^* \simeq \mathbb{R}^n$. For all $v \in V$ and $\sigma \in V^* \simeq R^n$ then:

$$\begin{aligned} \langle \sigma, v \rangle &= \sigma^{\mathrm{T}} a \\ \langle \hat{\sigma}, \hat{v} \rangle &= \frac{1}{2} \mathrm{trace}(\hat{\sigma}^{\mathrm{T}} \hat{v}). \end{aligned} \tag{A.4}$$

A.2. Metric Properties of SO(3)

On a general manifold M, a positive definite quadratic form $\langle\langle \xi_1, \xi_2 \rangle\rangle_{T_x M}$ defined on any tangent space $T_x M \ni \xi_1, \xi_2$ (the space tangent to M in $x \in M$) is called a Riemannian metric [37]. In mechanics a metric is tightly linked to the definition of kinetic energy [41]. Lie groups are, by definition, manifolds and, therefore, are entitled to posses metric properties. Lie groups, in particular $SO(3)$, are structured in such a way that some metrics naturally arise. Natural means that it does not depend on a particular choice of coordinates. A left-invariant metrics does not depend on the choice of the space frame, i.e., it only needs to be defined on the Lie algebra and then it can be left-translated to the tangent space at any other group element:

$$\langle\langle R\hat{a}, R\hat{c} \rangle\rangle_{T_R SO(3)} = \langle\langle \hat{a}, \hat{c} \rangle\rangle_{so(3)},$$

where $R \in SO(3)$ and $\hat{a}, \hat{c} \in so(3)$.

Still, there many choices for a metrics in the Lie algebra, as many as there are positive definite matrices P:

$$\langle\langle \hat{a}, \hat{c} \rangle\rangle_{so(3)} \triangleq a^{\mathrm{T}} P c,$$

where $a, c \in \mathbb{R}^3$ correspond to $\hat{a}, \hat{c} \in so(3)$ as in (A.1). However, there only exists one choice (up to a coefficient [34, 37, 39, 41]) when the metrics needs to be bi-invariant (i.e., both right- and left-invariant):

$$\langle\langle \hat{a}, \hat{c} \rangle\rangle_{so(3)} \triangleq a^{\mathrm{T}} I c = a^{\mathrm{T}} c = \langle a, c \rangle, \tag{A.5}$$

where I is the 3×3 identity matrix.

Two main results provided in Ref. [34] are the existence of a natural norm (which measures the distance between R and the identity I) on $SO(3)$:

$$\|R\|_{SO(3)} = \langle\langle \hat{\phi}_R, \hat{\phi}_R \rangle\rangle_{so(3)}^{1/2} = \|\phi_R\|_{\mathbb{R}^3} \tag{A.6}$$

and a formula for computing its time derivative on the Lie algebra $so(3)$:

$$\frac{1}{2} \frac{\mathrm{d}}{\mathrm{d}t} \|R(t)\|_{SO(3)} = \langle\langle \hat{\phi}_R, R^{\mathrm{T}} \dot{R} \rangle\rangle_{so(3)}, \tag{A.7}$$

where $\hat{\phi}_R \in so(3)$, also referred to as $\log R$, is defined as the angular velocity that takes the rigid body from I to $R \in SO(3)$ in one time unit; see Ref. [39] for details on the logarithmic map:

$$\hat{\phi}_R = \log R = \frac{\theta_R}{2\sin\theta_R}(R - R^{\mathrm{T}}), \tag{A.8}$$

where for $\mathrm{trace}(R) \neq -1$, θ_R satisfies $1 + 2\cos\theta_R = \mathrm{trace}(R)$ and $\|\phi_R\|^2 = \theta_R^2$, and the Rodrigues' formula:

$$R = \exp(\hat{\phi}_R) = I + \alpha_R\hat{\phi}_R + \beta_R\hat{\phi}_R^2, \tag{A.9}$$

where $\alpha_R = \|\phi_R\|^{-1}\sin\|\phi_R\|$ and $\beta_R = (1 - \cos\|\phi_R\|)\|\phi_R\|^{-2}$.

Appendix B. Proof of Main Theorem and Related Lemmas

B.1. Proof of Lemma 1

Monoaxial sensors are characterized by a sensitive axis along which the components of a vector field (e.g., angular velocity, gravitational field, geomagnetic field, etc.) can be measured. A body frame $\mathcal{B}$ identifies three orthogonal directions on a rigid body. Monoaxial sensors are, by construction, assembled on a rigid body in such a way that their sensitive axis coincides with one of axes defined by $\mathcal{B}$.

By construction, a set of three monoaxial gyroscopes provides the components of the angular velocity with respect to the body frame $\mathcal{B}$, i.e., $\hat{\omega}_{\mathrm{gyr}} = \hat{\omega} = R^{\mathrm{T}}\dot{R}$.

As for the effect of an arbitrary rotation R on the components of the fields $\vec{v}_1, \vec{v}_2, \ldots, \vec{v}_N$ as these are measured in the body frame, when the body frame coincides with the space frame $\mathcal{S}_0$, by Definition 1, the field components are given by v_{0i} both in the body frame and in the space frame, i.e., the identity matrix I relates the field components in $\mathcal{S}_0$ with the measured components in the body frame. For an arbitrary orientation R of the body with respect to $\mathcal{S}_0$ the components of the fields as measured by the sensors relative to the body can be expressed as $v_i = R^{\mathrm{T}}v_{0i}$.

B.2. Proof of Lemma 2

First, a proof of (9) is provided which mainly makes use of the following identities on $so(3)$ which hold for all $x, y \in \mathbb{R}^3$:

$$\begin{gathered}
\hat{x} = -\hat{x}^{\mathrm{T}} \\
\hat{x}^2 = \hat{x}^{2\mathrm{T}} \\
\hat{x}\hat{y} = yx^{\mathrm{T}} - x^{\mathrm{T}}yI \\
\hat{x}\hat{y} - \hat{y}\hat{x} = \widehat{(x \times y)} \\
\hat{x}\hat{y}^2 + \hat{y}^2\hat{x} = -\|y\|^2\hat{x} - x^{\mathrm{T}}y\hat{y} \\
\hat{x}\hat{y}\hat{x} = -x^{\mathrm{T}}y\hat{x} \\
\hat{x}^2\hat{y}\hat{x} - \hat{x}\hat{y}\hat{x}^2 = 0 \\
\hat{x}^2\hat{y}\hat{x}^2 = x^{\mathrm{T}}y\|x\|^2\hat{x},
\end{gathered} \tag{B.1}$$

where $x^{\mathrm{T}}y$ is the dot product in $\mathbb{R}^3$.

Express E as a function of ϕ_E (where $\hat{\phi}_E = \log(E)$) *via* the Rodrigues' formula (A.9):

$$E = \exp(\hat{\phi}_E) = I + \alpha_E \hat{\phi}_E + \beta_E \hat{\phi}_E^2 \tag{B.2}$$

$$\text{where } \begin{cases} \alpha_E = \frac{\sin\|\phi_E\|}{\|\phi_E\|} \\ \beta_E = \frac{1-\cos\|\phi_E\|}{\|\phi_E\|^2}. \end{cases} \tag{B.3}$$

Using identities (B.1) and the fact that $\beta_E - \alpha_E^2 - \beta_E^2\|\phi_E\|^2 = -\beta_E$, expand the term $-E^{\mathrm{T}}\widehat{\omega}E + \widehat{\omega}$ after substituting (B.2) as:

$$\begin{aligned} -E^{\mathrm{T}}\widehat{\omega}E + \widehat{\omega} &= \alpha_E(\widehat{\phi_E \times \omega}) + \beta_E\|\phi_E\|^2\widehat{\omega} + \phi_E^{\mathrm{T}}\omega(\beta_E - \alpha_E^2 - \beta_E^2\|\phi_E\|^2)\hat{\phi}_E \\ &= \alpha_E(\widehat{\phi_E \times \omega}) + \beta_E\|\phi_E\|^2\widehat{\omega} - \beta_E(\phi_E^{\mathrm{T}}\omega)\hat{\phi}_E. \end{aligned}$$

It is now straightforward verifying (B.4):

$$\begin{aligned} &\langle\langle \log(E), -E^{\mathrm{T}}\widehat{\omega}E + \widehat{\omega}\rangle\rangle_{so(3)} \\ &\quad = \big\langle\big\langle \hat{\phi}_E, \alpha_E(\widehat{\phi_E \times \omega}) + \beta_E\|\phi_E\|^2\widehat{\omega} - \beta_E(\phi_E^{\mathrm{T}}\omega)\hat{\phi}_E \big\rangle\big\rangle_{so(3)} \\ &\quad = \phi_E^{\mathrm{T}}\big(\alpha_E(\phi_E \times \omega) + \beta_E\|\phi_E\|^2\omega - \beta_E(\phi_E^{\mathrm{T}}\omega)\phi_E\big) \\ &\quad = 0 + \beta_E\|\phi_E\|^2(\phi_E^{\mathrm{T}}\omega) - \beta_E(\phi_E^{\mathrm{T}}\omega)\|\phi_E\|^2 \\ &\quad = 0, \end{aligned} \tag{B.4}$$

which proves (9).

Given the tracking error definition $E = R^{\mathrm{T}}R^*$, the error dynamics are easily computed as:

$$\dot{E} = \dot{R}^{\mathrm{T}}R^* + R^{\mathrm{T}}\dot{R}^*.$$

Since $R^{*\mathrm{T}}\dot{R}^* = \widehat{\omega} = R^{\mathrm{T}}\dot{R}$, it can be verified that:

$$E^{\mathrm{T}}\dot{E} = -E^{\mathrm{T}}\widehat{\omega}E + \widehat{\omega}.$$

Rather than $E(t)$, we are interested in $\|E(t)\|$ and from (A.7) we can write:

$$\begin{aligned} \frac{\mathrm{d}}{\mathrm{d}t}\|E(t)\|_{SO(3)} &= \langle\langle \hat{\phi}_E, E^{\mathrm{T}}\dot{E}\rangle\rangle_{so(3)} \\ &= \langle\langle \hat{\phi}_E, -E^{\mathrm{T}}\widehat{\omega}E + \widehat{\omega}\rangle\rangle_{so(3)} \\ &= 0, \end{aligned}$$

and, therefore:

$$\|E(t)\|_{SO(3)} = \text{constant} = \|E(0)\|_{SO(3)}.$$

B.3. Proof of Theorem 1

Considering that $\widehat{\omega}_{\text{gyr}} = \widehat{\omega}$ by (7), the whole system (10) can be conveniently rewritten as:

$$\dot{R}^* = R^* \left(\widehat{\omega} + \sum_{i=1}^{N} k_i [\hat{v}_i, \hat{v}_i^*] \right), \tag{B.5}$$

where (A.3) was used to rewrite the cross-product in $\mathbb{R}^3$ in terms of the Lie commutator in $so(3)$.

Following Ref. [34], define the estimation error E as in (8) and consider its time derivative $\dot{E} = \dot{R}^{\mathrm{T}} R^* + R^{\mathrm{T}} \dot{R}^*$. Now use (B.5) to write the dynamics of estimation error as:

$$\begin{aligned}
E^{\mathrm{T}} \dot{E} &= R^{*\mathrm{T}} R \dot{R}^{\mathrm{T}} R^* + R^{*\mathrm{T}} R R^{\mathrm{T}} \dot{R}^* \\
&= R^{*\mathrm{T}} R \dot{R}^{\mathrm{T}} R^* + R^{*\mathrm{T}} \dot{R}^* \\
&= R^{*\mathrm{T}} R \dot{R}^{\mathrm{T}} R^* + \widehat{\omega} + \sum_{i=1}^{N} k_i [\hat{v}_i, \hat{v}_i^*] \\
&= R^{*\mathrm{T}} R \dot{R}^{\mathrm{T}} R R^{\mathrm{T}} R^* + \widehat{\omega} + \sum_{i=1}^{N} k_i [\hat{v}_i, \hat{v}_i^*] \\
&= E^{\mathrm{T}} \dot{R}^{\mathrm{T}} R E + \widehat{\omega} + \sum_{i=1}^{N} k_i [\hat{v}_i, \hat{v}_i^*].
\end{aligned}$$

Note that $\frac{\mathrm{d}}{\mathrm{d}t}(R^{\mathrm{T}} R) = \frac{\mathrm{d}}{\mathrm{d}t}(I) = 0$ implies that $\dot{R}^{\mathrm{T}} R + R^{\mathrm{T}} \dot{R} = 0$ and, therefore:

$$E^{\mathrm{T}} \dot{E} = -E^{\mathrm{T}} \widehat{\omega} E + \widehat{\omega} + \sum_{i=1}^{N} k_i [\hat{v}_i, \hat{v}_i^*]. \tag{B.6}$$

In order to prove stability, as in Ref. [34], the natural norm on $SO(3)$ defined in (A.6) is chosen as a positive-definite candidate Lyapunov function $W(E)$, i.e.:

$$W(E) \triangleq \frac{1}{2} \|E\|_{SO(3)} = \frac{1}{2} \langle\!\langle \log(E), \log(E) \rangle\!\rangle_{so(3)}^{1/2}, \tag{B.7}$$

where $\log(E) = \hat{\phi}_E \in so(3)$ is defined in (A.8), while $\langle\!\langle \cdot, \cdot \rangle\!\rangle_{so(3)}$ is the bi-invariant metric defined in (A.5).

The time derivative of $W(E)$ can be computed *via* (A.7) as:

$$\dot{W}(E) = \frac{1}{2} \frac{\mathrm{d}}{\mathrm{d}t} \|E\|_{SO(3)} = \langle\!\langle \log(E), E^{\mathrm{T}} \dot{E} \rangle\!\rangle_{so(3)}.$$

Substituting (B.6):

$$\dot{W}(E) = \langle\!\langle \log(E), -E^{\mathrm{T}} \widehat{\omega} E + \widehat{\omega} \rangle\!\rangle_{so(3)} + \left\langle\!\!\left\langle \log(E), \sum_{i=1}^{N} k_i [\hat{v}_i, \hat{v}_i^*] \right\rangle\!\!\right\rangle_{so(3)}. \tag{B.8}$$

As shown in Lemma 2, the first term in the right side of the last equation is always zero and, therefore:

$$\dot{W}(E) = \left\langle\!\!\left\langle \log(E), \sum_{i=1}^{N} k_i [\hat{v}_i, \hat{v}_i^*] \right\rangle\!\!\right\rangle_{so(3)}. \tag{B.9}$$

Equation $v_i = R^{\mathrm{T}} v_{0i}$ from (7) and equation $v_i^* = R^{*\mathrm{T}} v_{0i}$ from (10) lead to:

$$v_i = E v_i^*,$$

therefore, recalling (A.3) and (A.5), $\dot{W}(E)$ can be written in terms of $\mathbb{R}^3$ vectors as:

$$\dot{W}(E) = \phi_E^{\mathrm{T}} \left(\sum_{i=1}^{N} k_i ((E v_i^*) \times v_i^*) \right) = \sum_{i=1}^{N} k_i \phi_E^{\mathrm{T}} ((E v_i^*) \times v_i^*).$$

In order to study the sign of $\dot{W}(E)$, it is convenient to express E as a function of ϕ_E *via* the Rodrigues' formula (A.9):

$$E = \exp(\hat{\phi}_E) = I + \alpha_E \hat{\phi}_E + \beta_E \hat{\phi}_E^2 \tag{B.10}$$

$$\text{where} \begin{cases} \alpha_E = \frac{\sin \|\phi_E\|}{\|\phi_E\|} \\ \beta_E = \frac{1 - \cos \|\phi_E\|}{\|\phi_E\|^2}, \end{cases} \tag{B.11}$$

and rewrite:

$$\dot{W}(E) = \sum_{i=1}^{N} k_i \phi_E^{\mathrm{T}} \big((v_i^* + \alpha_E \hat{\phi}_E v_i^* + \beta_E \hat{\phi}_E^2 v_i^*) \times v_i^* \big). \tag{B.12}$$

Consider the following identities for all $\phi, v \in \mathbb{R}^3$:

$$\begin{gathered} v \times v = 0 \\ (\hat{\phi} v) \times v = (\phi^{\mathrm{T}} v) v - \|v\|^2 \phi \\ \phi^{\mathrm{T}} ((\hat{\phi}^2 v) \times v) = 0, \end{gathered}$$

which allow writing:

$$\begin{aligned} \dot{W}(E) &= \sum_{i=1}^{N} k_i \phi_E^{\mathrm{T}} ((\alpha_E \hat{\phi}_E v_i^*) \times v_i^*) \\ &= \sum_{i=1}^{N} k_i \alpha_E \big((\phi_E^{\mathrm{T}} v_i^*)^2 - \|v_i^*\|^2 \|\phi_E\|^2 \big). \end{aligned} \tag{B.13}$$

Recalling that $\phi_E^{\mathrm{T}} v_i^* = \|\phi_E\| \|v_i^*\| \cos\theta_i$ (by the dot product in $\mathbb{R}^3$, where θ_i is the angle between ϕ_E and v_i^*) and that $\alpha_E = \sin \|\phi_E\| / \|\phi_E\|$ from (B.10), we can write:

$$\dot{W}(E) = -\sum_{i=1}^{N} k_i \sin \|\phi_E\| \|\phi_E\| \|v_i^*\|^2 (1 - \cos^2 \theta_i), \tag{B.14}$$

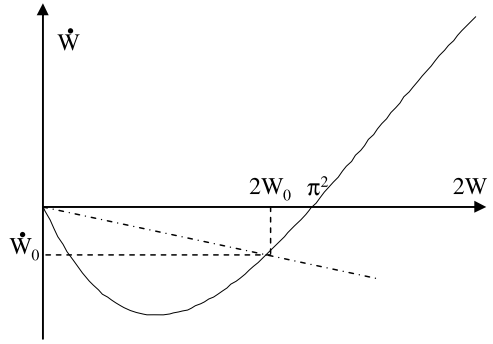

Figure B.1. Plot of the function $\dot{W} = -\gamma\sqrt{2W}\sin\sqrt{2W}$ *versus* $2W$.

moreover, since $v_i^* = R^{*\mathrm{T}} v_{0i}$ and $R^* \in SO(3)$ then $\|v_i^*\| = \|v_{0i}\|$, and then:

$$\dot{W}(E) = -\|\phi_E\| \sin\|\phi_E\| \sum_{i=1}^{N} k_i \|v_{0i}\|^2 (1 - \cos^2\theta_i). \tag{B.15}$$

Consider the following inequality:

$$\sum_{i=1}^{N} k_i \|v_{0i}\|^2 (1 - \cos^2\theta_i) \geqslant \sum_{i=1}^{2} k_i \|v_{0i}\|^2 (1 - \cos^2\theta_i),$$

since $k_i > 0$. θ_i represents the alignment between ϕ_E, and v_i and since v_1 and v_2 are assumed independent in (6), ϕ_E can never be aligned, at the same time, with both v_1 and v_2. Therefore, θ_1 and θ_2 can never be zero at the same time. This implies that $\exists\gamma > 0$ such that:

$$\sum_{i=1}^{N} k_i \|v_{0i}\|^2 (1 - \cos^2\theta_i) \geqslant \sum_{i=1}^{2} k_i \|v_{0i}\|^2 (1 - \cos^2\theta_i) \geqslant \gamma > 0,$$

therefore, recalling from (B.7) that $W(E) = 1/2\|\phi_E\|^2$, we can write:

$$\dot{W}(E) \leqslant -\gamma\sqrt{2W(E)}\ \sin\sqrt{2W(E)}, \tag{B.16}$$

or, simplifying the notation:

$$\dot{W} \leqslant -\gamma\sqrt{2W}\ \sin\sqrt{2W}. \tag{B.17}$$

For any initial configuration $E(0)$ such that $\mathrm{trace}(E(0)) \neq -1$, the logarithmic map (A.8) guarantees that $\|\phi_E\| < \pi$, i.e., the following holds for $W_0 \triangleq 2W(E(0))$:

$$0 \leqslant 2W_0 < \pi^2.$$

In such an interval, as shown in Fig. B.1, a linear upper bound can always be found such that:

$$\dot{W} \leqslant -\lambda\sqrt{2W}\sin\sqrt{2W} \leqslant \frac{\dot{W}_0}{W_0} W = -\eta W,$$

where $\eta > 0$ since $\dot{W}_0 = \dot{W}(E(0)) < 0$. This finally proves convergence since the linear upper bound can easily be integrated, leading to:

$$0 < W(t) \leqslant W_0 \mathrm{e}^{-\eta t} \quad \Rightarrow \quad \lim_{t\to\infty} W(t) = 0.$$

Since $W(t) = W(E(t))$ measures the distance between $E = R^{\mathrm{T}}(t)R^*(t)$ and $I \in SO(3)$, then:

$$\lim_{t\to\infty} R^{\mathrm{T}}(t)R^*(t) = I.$$

About the Authors

Domenico Campolo is currently a Senior Researcher at Università Campus Bio-Medico in Rome, Italy. He received his Laurea Degree from the University of Pisa, in 1998, and the Diploma Degree from Scuola Superiore Sant'Anna, in 1999. In 2002, he earned his PhD in Micro-Engineering from Scuola Superiore Sant'Anna, Pisa, while working at MiTech Lab (currently the CRIM Lab). During the Fall 1998 he was working at the EECS Department of ZheJiang University, HangZhou, P. R. China, as a Visiting Graduate Student. In the period 2000–2003, he was at UC-Berkeley, USA, as a Visiting Scholar and, after 2002, as a Post-Doc working on the MFI (Micromechanical Flying Insect) project. His research interests include mechatronic technologies with application to the new emerging fields of Phenomics and Neuro-Developmental Engineering, in both animal and human models; biomimetic microrobotics, including: design, fabrication, development and control of biologically inspired smart actuators and sensors; micro/nano-manipulation; and micro/nano-fabrication. He is co-author of more than 35 peer-reviewed papers in international journals and conference proceedings.

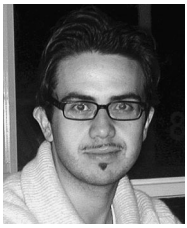

Luca Schenato received the DE degree in Electrical Engineering from the University of Padova, in 1999 and the PhD degree in Electrical Engineering and Computer Sciences from UC Berkeley, in 2003. From January 2004 to August 2004 he was a Post-doc at UC Berkeley. Currently, he is Associate Professor at the Information Engineering Department at the University of Padova. His interests include swarm robotics and biomimetic locomotion, networked control systems, wireless sensor networks, and distributed control. He was awarded the 2004 Researchers Mobility Fellowship by the Italian Ministry of Education, University and Research (MIUR), and the 2006 Eli Jury Award at UC Berkeley.

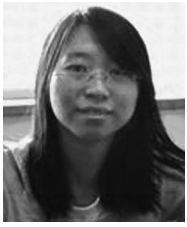

Lijuan Pi is currently a Graduate Student at the Mechanical Engineering Department of the University of Delaware. She works the MicroRobotics Lab.

Xinyan Deng received her BS degree from the Department of Automation of Tianjin University, China. She received her PhD degree from the Mechanical Engineering Department of the University of California at Berkeley in 2004. Since then she has been an Assistant Professor at the Department of Mechanical Engineering at the University of Delaware. Her research interest is on the principles of aerial and aquatic locomotion in animals and robots, including experiment fluid mechanics, dynamics and control, and bio-inspired systems. She received an NSF CAREER Award in 2006.

Eugenio Guglielmelli received the Laurea Degree (Master) in Electronics Engineering, and the PhD in Elctronics, Telecommunications and Computer Science (Biomedical Robotics track) from the University of Pisa, Italy, in 1991 and 1995. He is currently Associate Professor of Bioengineering at Università Campus Bio-Medico, Rome, Italy, where he serves as the Head of the Laboratory of Biomedical Robotics and Biomicrosystems. From 1991 to 2004, he worked with Professor Paolo Dario at the Advanced Robotics Technology & Systems Laboratory (ARTS Lab) of the Scuola Superiore Sant'Anna, Pisa, Italy, that he directed from 2002 to 2004. His main current research interests are in the fields of human-centred robotics, biomechatronic design and biomorphic control of robotic systems, and in their application to robot-mediated motor therapy, assistive robotics and neurorobotics. He is author/co-author of more than 150 papers appearing in peer-reviewed international journals, conference proceedings and books. He currently serves as Associate Editor of the *IEEE Robotics and Automation Magazine* and on the Editorial Board of the international journal on *Applied Bionics and Biomechanics*. He has been Guest Co-Editor of the Special Issues on Rehabilitation Robotics of the *IEEE Transactions on Robotics* and of the *International Journal Autonomous Robots*, and also of the Special Issue on Robotics Platforms for Neuroscience of the RSJ international journal *Advanced Robotics*. He is principal investigator/partner of several national and international projects in the area of biomedical robotics. He is member of the IEEE Robotics & Automation Society, IEEE Engineering in Medicine & Biology Society and Society for Neuroscience. He is currently Associate Vice-President for Technical Activities of the IEEE Robotics & Automation Society (RAS) and he also served as Co-chair of the Technical Committee on Rehabilitation and Assistive Robotics (2004–2007) and as RAS Secretary (2002–2003) of the same society. He was/is member of the Organizing Committees of HURO1998, ICAR2003, IROS2004, IFAC/SYROCO2006, ICRA2007 and ROMAN2009, and of the Programme Committees of several international conferences, workshops and symposia.